Letters on materials 7 (4), 2017 pp. 447-451 www.lettersonmaterials.com

DOI: 10.22226/2410-3535-2017-4-447-451 PACS 81.07.Bc, 61.72.Cc

Influence of Zr on intergranular corrosion of cast and cryorolled D16 aluminum alloy

M. V. Markushev†, S. V. Krymskiy, R. R. Ilyasov, E. V. Avtokratova,

A. A. Khazgalieva, O. Sh. Sitdikov

†mvmark@imsp.ru

Institute for Metals Superplasticity Problems of RAS, Khalturin St. 39, Ufa, 450001, Russia

Effects of severe plastic deformation by isothermal cryorolling at a temperature of liquid nitrogen with a strain of $e \sim 2$ and subsequent aging on structure, hardness and resistance to intergranular corrosion (IGC) of the preliminary quenched ingots of the conventional and Zr modified composition of D16 aluminum alloy, were investigated. It was found that both the alloys in the natural aged condition demonstrate slight effect on IGC resistance. It was caused by low difference in electrochemical potentials between the matrix and Guinier-Preston-Bagaratsky zones. Artificial aging at 190°C for 12 hrs to the maximum strength (T1 route) led to strong decrease in IGC resistance of both rolled and non-rolled states of the alloys due to precipitation of strengthening phases. Modification the D16 alloy composition via substitution of Mn by twice less amounts of Zr and decrease in impurity contents had a minor influence on its structure and hardness in the initial and rolled conditions. However, it significantly enhanced corrosion resistance, reducing its depth and intensity, in both naturally and artificially aged conditions. It was concluded that the main factors, determining the alloy microstructure changes, mechanical and corrosion behavior, are the volume fraction, morphology, and spatial distribution of second phases — excess phases and precipitates.

Keywords: aluminum alloy, intergranular corrosion, severe plastic deformation, structure, aging.

1. Introduction

During last decades, aluminum alloys occupied the leading position among other structural materials in transport, energy, building and other industries. Herewith, according to [1], about 30% of their failure is caused by corrosion, frequently having a character of intergranular corrosion (IGC). It is well known that IGC driving force is conditioned by the difference in electrochemical potentials on the border between the alloy matrix-solid solution of main alloying elements in aluminum, and intermetallic second phases. Generally, the larger is a particle and the lesser is its coherency with the matrix, the higher is the difference of these potentials [2,3]. Besides, it is well documented that the main IGC parameters — depth and intensity of corrosion, are strongly dependent on the alloy microstructure and phase composition, that is on the grain and subgrain size [4 – 6]; structure and fraction of high and low-angle boundaries [7 – 13]; nature, morphology and distribution of primary and secondary phases [14 – 16]; width of precipitate free zones (PFZs) [17,18] and etc.

Developing new alloys and methods of their strengthening have caused appreciable interest to severe straining (with $e > 2 – 3$) at low homological (cryogenic) temperatures. Such a processing of pure metals and alloys usually results in well-developed deformation structures, involving nanocrystalline structures, and could be accompanied by their enhanced strength, as also of other physical and mechanical properties [19 – 24]. Meanwhile, it should be noted, that any cold deformation, even to conventional low strains, ambiguously affects aluminum alloys IGC resistance [2,11]. The cause is that straining commonly leads to simultaneous, but complex and multifactorial changes in structure and phase parameters, involving those, mentioned above. For example, it was found in [26] that cryorolling increased IGC intensity of commercial purity aluminum due to grain refinement and work hardening. At the same time, in [18] cryorolled and aged at 150°C Al-Zn-Mg alloy demonstrated the increased density of corrosion lesions with decreasing their depth. This was due to some spreading of strings of excess phases and absence of PFZs along grain boundaries, which were the character features of the alloy structure in the initial, non-rolled condition.

Microalloying of aluminum alloys by rare earth/transition metals (TM) was found to be an effective way of their microstructure and property control [27]. One of the main effects is caused by grain refinement under the alloy processing, starting from cast structure of an ingot. Another is conditioned by the alloy strengthening due to formation of high densities of disperse coherent aluminides. The most effective are complex additions of few TMs, as Zr, Sc, Mn and Cr, significantly enhancing, for instance, the IGC resistance of age-hardenable Al-Zn-Mg-Cu alloys [28]. Herewith, their effect on dispersion strengthening is summarized with work hardening effect, conditioned by the formation of nanosized precipitates strongly inhibiting recrystallization of the matrix.

The aim of the present study is to analyze the effect of the D16 alloy composition modification, via substitution of Mn by Zr and decrease in the impurity (Fe and Si) contents, on structure-property relations in the initial cast, cryorolled and further natural and artificial aged states, and to discuss their corrosion behavior.

2. Material and procedure

Plates of 5 mm in thickness cut out from cast ingots of standard and modified D16 alloy (Table 1), were preliminary solution treated at 505°C and water quenched (Q). Further cryorolling (CR) was performed to the strains of $e \sim 2.0$ in isothermal conditions at a temperature of liquid nitrogen. Finally, the alloys were naturally or artificially aged (NA and AA) in accordance to T and T1 conventional routes at 20°C for 6 days, and at 190°C for 12 hrs, consequently. The grain structure of the aluminum matrix, as well as the second phases (coarse particles of excess phases and disperse precipitates) were examined by optical metallography, transmission and scanning electron microscopy (OM, TEM and SEM). Objects for analyses were prepared by standard procedures, involving jet electro-polishing in 20% solution of nitric acid in methanol. The alloy microhardness (HV) was measured using Vickers indenter with a load of 1 N and loading time 10 sec. The resistance to intergranular corrosion was tested on samples exposed in 3% sodium chloride and 1% hydrochloric acid water solution during 24 hrs. The average depth and intensity of corrosion attack were determined by SEM measurements along contact surface-cross section of a sample (for rolled sheets — in rolling direction).

3. Results and discussion

OM and SEM analyses indicated that the initial microstructure of both the alloy compositions was presented by coarse, with the average size of 300 – 400 μm, grains and coarse, up to few microns in thick excess phases, mainly distributed along the grain boundaries, and near homogeneously distributed precipitates of aluminides of transition metals inside the alloy matrix (Figs. 1 and 2). That is, the alloy of standard composition contained coarse excess $Al_{15}Si_5(CuFeMn)_3$ and S (Al_2CuMg) phases with a volume fraction of 2.4 ± 0.1%, predominantly aligned at grain boundaries, while inside its grains there were TEM detectable disperse rod-shaped Mn-rich T-phases ($Al_{20}Cu_2Mn_3$) 50 – 200 nm in length (Fig. 3). Initial structure of the modified alloy consists of θ (Al_2Cu) excess phases of less volume fraction 1.1 ± 0.1% and sizes. Besides, inside the grain body and at the boundaries there were observed Al_3Zr coherent precipitates of 10 – 50 nm in diameter and higher densities (Figs. 3).

Cryorolling of both the alloys led to elongation of initial grains and formation of fibered structure with a thickness of fibers ~100 – 200 μm (Fig. 2b, d). Inside the fibers there were formed the well-developed, cellular structures with a cell size of ~0.4 – 0.5 μm (Fig. 3). Rolling also resulted in slight decrease in the mean volume fraction of excess phases to 2.3 ± 0.1 and 0.9 ± 0.1% in standard and modified alloy, consequently, with slight decrease in their size and homogeneity of distribution inside the sheets. The latter resulted in formation of strings along the fiber boundaries. After further natural and artificial aging the alloys deformation structures remained cellular ones (Fig. 3 c – f). However, they became more equilibrium, especially after aging at elevated temperature, due to static recovery, resulting in some insignificant changes in cell size and defectiveness of grain structure (dislocation density). Moreover, simultaneously there was occurred decomposition of the preliminary supersaturated by Cu and Mg aluminum solid solution with formation at low aging times Guinier-Preston-Bagaratsky zones (GPBZ), which were further transformed in non-equilibrium S′ and S″ phases. Aging also resulted in transformation of the alloys highly work-hardened structure into a more equilibrium one due to

Table 1. Chemical composition of the alloys investigated.

Alloy	Alloying elements, wt. %						
	Al	Cu	Mg	Mn	Zr	Fe	Si
Standard	balance	4.2	1.3	0.5	–	0.35	0.25
Modified	balance	4.4	1.1	0.01	0.22	0.02	–

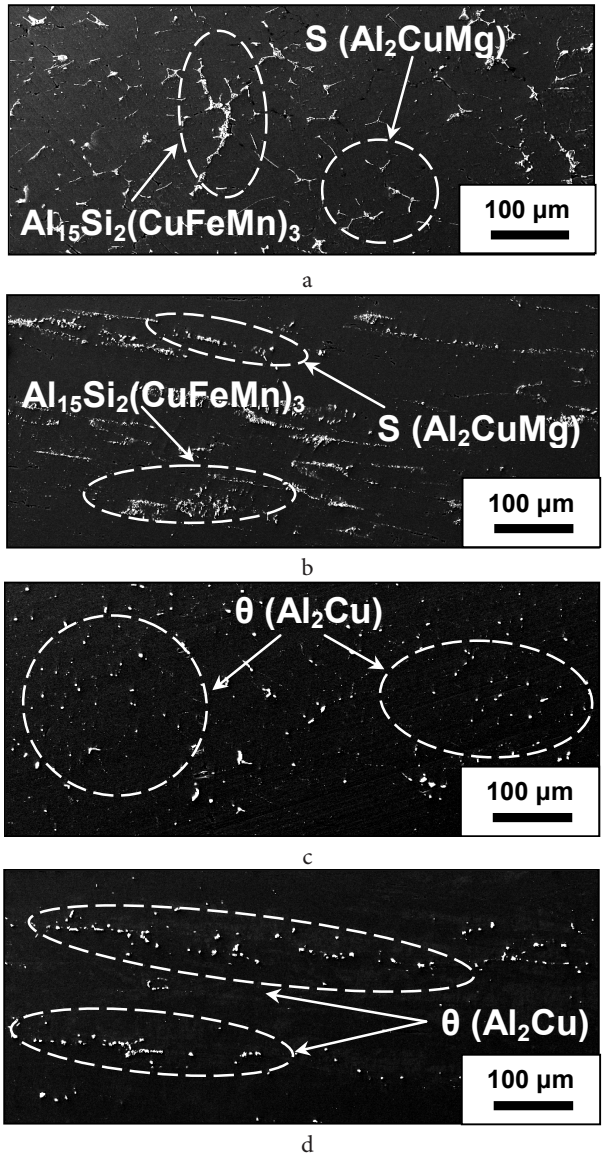

Fig. 1. SEM images of excess phases in standard (a, b) and modified (c, d) alloys before (a, c) and after cryorolling (b, d) (rolling plane).

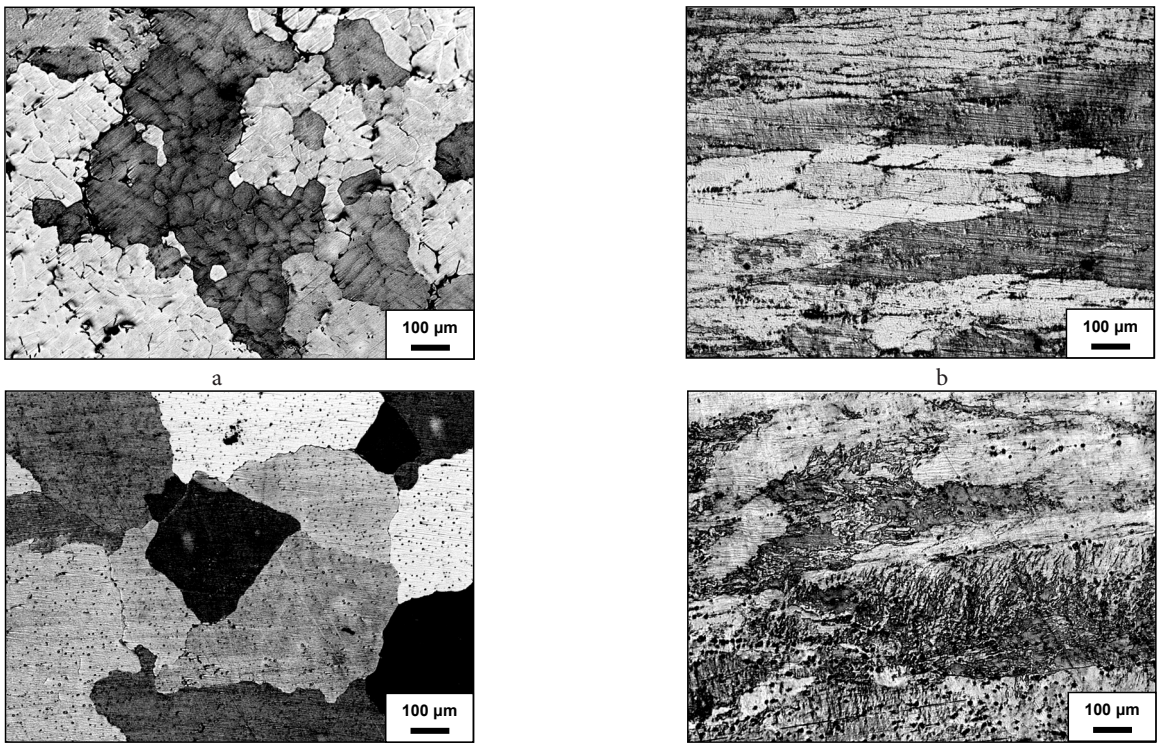

Fig. 2. OM structures of standard (a, b) and modified (c, d) alloys in quenched (a, c), cryorolled and naturally aged (b, d) conditions (rolling plane).

recovery and recrystallization (Fig. 3 c – f). At that in AA alloys it became more complex and inhomogeneous owing to incompleteness of recrystallization, leading to even partial substitution of deformation cells by areas with recovered subgrains and areas of new grains. Besides, inside and along the grain and subgrain boundaries (consequently, recovered and recrystallized structures) nanoprecipitates of different nature and morphology were formed (see more details in [21,22]). In general, such a structure can be characterized as bimodal, consisting of recovered areas with needle (disc)-like S-phase precipitates with a thickness of 2 – 10 nm and length up to ~100 nm, and areas of nano/ultrafine (sub)grains with compact slightly elongated precipitates of 10 – 50 nm in size. Two main factors could be caused for such a structure formation. The first one is intensification of growth (coagulation) of strengthening phases in a highly work-hardened (defect) matrix, the second one — changes in precipitate morphology (predominantly in phase shape and structure of interphase boundary) are caused by nucleation and growth of precipitates in simultaneously changing structure of the surrounding matrix due to recrystallization. Therefore, artificial aging of cryorolled alloys led to formation of a multilevel nanostructure, described by two nano-sized phase constituents — crystallites of the matrix and precipitates, their volume fractions and morphology.

It was found that the microhardness of both the alloys before rolling was almost equal. Moreover, their further straining and aging resulted in significant, but near the same alloys hardening (Table 2), testifying absence of the effect of the alloy composition modification. It is necessary to note that such a behavior was found for both rolled alloys after both natural and artificial aging. The light distinction was found only in the level of their softening due to simultaneous occurrence of static recovery, continuous static recrystallization and aluminum solid solution decomposition, forming multilevel nanostructure described above. This softening was a bit higher in the modified alloy.

Analyses the samples cross sections, perpendicular to contact surface with the corrosive media of cryorolled and naturally aged alloys, revealed them to be commonly undamaged with numerical separate lesions (Fig. 4a, c). So, the parameters of their IGC had quite low values (Table 2). However, the depth of corrosion was about three and intensity one and a half times less in modified alloy. Such a behavior, virtually, could be caused by the difference in second phase structures only. In particular, by less density and size of excess phases of different composition on contact surfaces of specimen (Fig. 4a, c).

In contrast, the alloys conventional artificial aging led to the well-defined corrosion attacks, deeply spreading inside the specimens (Fig. 4b, d). The both alloy's samples were completely corroded, testifying 100% IGC intensity, and the depth of corrosion was the highest and also near two times deeper in the standard alloy. Its lesions predominantly developed along grain boundaries, connecting with strings of excess phases, and spread inside fibers along subgrain boundaries, forming dendrite-like structure. Distributions of damages along the contact surfaces were quite inhomogeneous and determined by the corresponding distances between strings of excess phases. In distinction, in the modified alloy, the lesion distributions were more homogeneous and had shorter continuous corrosion paths. It was caused by the absence of Mn and Fe-rich coarse phases and less developed string structure, being formed predominantly by spherical

and less in size particles of θ-phase. As a result near twice less IGC depth was observed in the modified alloy.

The alloys behavior found could be described as follows. It is well known that the main driving force for corrosion attack in 2xxx aluminum alloys is the difference in electrochemical potentials of volumes separated by (sub)grain boundaries. IGC develops predominantly along discrete and cathodic to its matrix grain, subgrain and interphase boundary areas, that is between grains and subgrains of aluminum solid solution and particles and precipitates, lying along their boundaries. Therefore, the more coherent with the matrix is the second phase, the less is the difference between their lattices and the less is IGC driving force. Also, IGC penetrates through discontinuous anode areas, as precipitate-free zones, usually forming under aging and lying along high-angle boundaries [2,4]. Thus, factors determining the alloys corrosion behavior, are commonly divided into structural and phase ones. The first group consists of factors, responding on structure of alloy matrix, the second — on structure of second phases. So, basing on the fact, that during the alloys processing both matrix and second phases have been subjected to simultaneous changes, it can be considered that its corrosion attack was synergy dependent on both types of factors. That is why, it is necessary to take into account their mutual influence in complex.

Judging by morphology of corrosion lesions, independently on regimes of alloys processing, and irrespectively of their composition, the corrosion attack is mainly developed at interphase boundaries, inside the areas adjacent to strings of excess phases (Fig. 4). Cryorolling led to thinning and subdivision of initial grains, decreasing the distances between these sites. Besides, the strings were formed with less interparticle spacing along and across rolling axis due to rupture of excess phases. As a result, density of particles along grain boundaries and on perpendicular contact surface increased.

Annealing of both cryorolled alloys at ambient temperature led to formation of GPBZ owing to aluminum solid solution decomposition. Because of their coherency with aluminum lattice, difference in their electrochemical potentials, consequently the IGC driving force, was low [2,4], causing insignificant corrosion penetration (Fig. 4, Table 2). Under artificial aging the main effect on alloys IGC resistance was reasoned by formation of metastable and stable phases. At that the compact non-coherent precipitates were found to form at aging in recrystallized areas, apparently intensifying the alloy corrosion damage. In that case the effect of Zr was the most pronounced as the zirconium aluminides were playing their main role — suppression of the matrix structure transformations, involving dislocation rearrangements. As a result, Zr addition significantly decreased the IGC depth. However, the main reason of such alloy behavior is caused by modified effect of Zr on the matrix microstructure and

Table 2. Microhardness, depth and intensity of intergranular corrosion (IGC) of pre-quenched, cryorolled and aged alloys.

Alloy	State	HV	IGC depth, μm	IGC intensity, %
Standard	Q	114	–	–
	Q + CR + NA	170	130	26
	Q + CR + AA	137	1419	100
Modified	Q	110	–	–
	Q + CR + NA	170	54	17
	Q + CR + AA	132	874	100

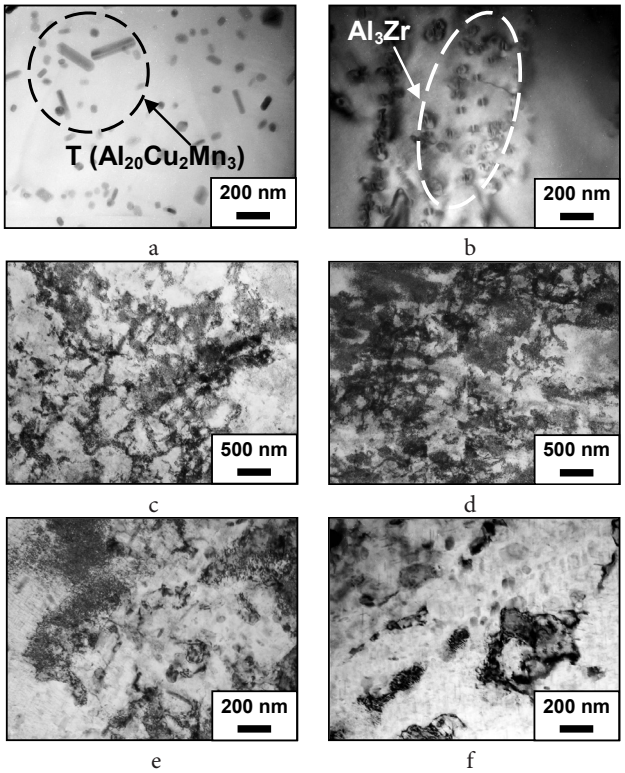

Fig. 3. TEM structures of the standard (a, c, e) and modified (b, d, f) alloys in pre-quenched (a, b), cryorolled and naturally (c, d) and artificially aged (e, f) conditions.

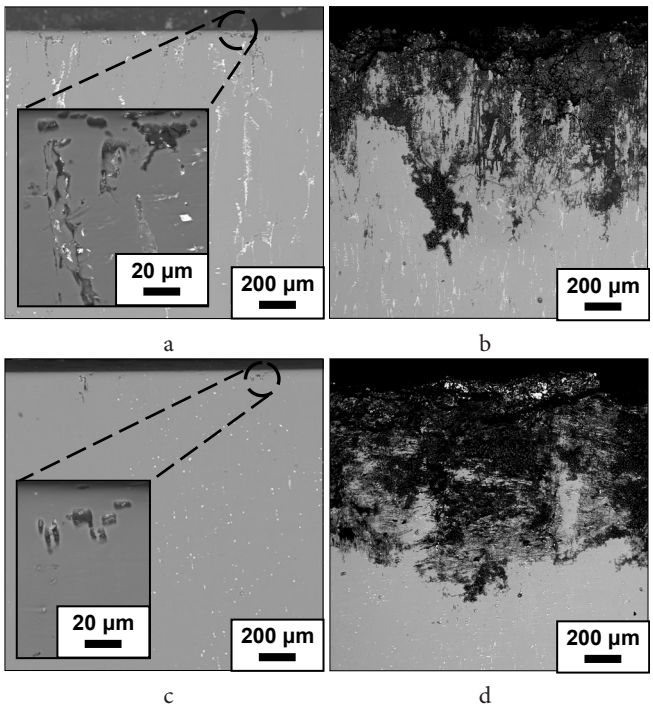

Fig. 4. SEM images of intergranular corrosion attack in the standard (a, b) and modified (c, d) alloys in cryorolled and naturally (a, c) and artificially aged (b, d) conditions.

absence of coarse excess $Al_{15}Si(CuFeMn)_3$ and S (Al_2CuMg) phases, forming strings at rolling. Actually, only compact spherical θ (Al_2Cu) phases were presented in Zr modified alloy, suppressing IGC because of absence of continuous corrosion paths.

4. Conclusions

Both alloy compositions in cryorolled and naturally aged conditions demonstrated quite high resistance to IGC parameters with near equal hardness. On the opposite, artificial aging under conventional T1 regime strongly increased depth and intensity of their corrosion. Herewith the alloy modification significantly improved the IGC depth at 100% intensity. The main reason of such alloy behavior is caused by reduced amount and sizes of coarse excess phases and their another composition.

Natural aging of CR alloys led to formation of GPBZ. Because of their coherency to matrix, difference in their electrochemical potential was low, causing slight effect on corrosion resistance. In case of artificial aging the main effect on alloy IGC was caused by metastable and stable S (Al_2CuMg) phases due to increased difference in the electrochemical potential at interphase boundary, leading to much intense attack compare with naturally aged condition.

So, the present study has shown that the effect of the alloy cryorolling on IGC is complex and conditioned by synergy of factors discussed above. This could lead to some unusual results. For instance, under post-deformation artificial aging, the alloy matrix recovery and recrystallization influenced the solid solution decomposition, changing its kinetics and sequence, as morphology and distribution of its products. Thus, during aging compact non-coherent precipitates of stable phases were formed in recrystallized areas and, apparently, intensified the alloy corrosion damage. At that Zr aluminides were acting as strong barriers of grain growth and dislocation rearrangements, consequently, decreasing the intensity of corrosion.

Thus, it could be concluded that the 2xxx alloy composition modification, involving substitution of Mn by twice less amounts of Zr and strong reduction in impurities, has a positive influence on its resistance to intercrystalline corrosion with no sense influence on its strength before and after severe straining via cryorolling.

Acknowledgements. The work was supported by the Russian Science Foundation (Grant No. 16-19-10152, processing the objects for investigation and microstructure analysis) and the Russian Foundation for Basic Research (Grant No. 16-38-00617, corrosion tests).

References

1. E. A. Starke, J. T. Staley. Prog. Aerosp. Sci. 32, 131 (1996).
2. V. S. Sinyavskiy, V. D. Valkov, V. D. Kalinin. Corrosion and protection of aluminum alloys. Moscow, Metallurgy. (1986) 368 p. (in Russian) [В. С. Синявский, В. Д. Вальков, В. Д. Калинин. Коррозия и защита алюминиевых сплавов. Москва, Металлургия. 1986. 368 с.]
3. http://aluminium.matter.org.uk/aluselect/default.asp
4. L. Beaunier. J. Phys. Coll. 43, 271 (1982).
5. K. D. Ralston, N. Birbilis, C. H. J. Davies. Scr. Mater. 63, 1201 (2010).
6. K. D. Ralston, D. Fabijanic, N. Birbilis. Electrochim. Acta. 56, 1729 (2011).
7. W. Wei, K. X. Wei, Q. B. Du. Mat. Sci. Eng. A. 454, 536 (2007).
8. M. K. Chung, Y. S. Choi, J. G. Kim, Y. M. Kim, J. Ch. Lee. Mat. Sci. Eng. A. 366, 282 (2004).
9. A. Balyanov, J. Kutnyakova, N. A. Amirkhanova, V. V. Stolyarov, R. Z. Valiev, X. Z. Liao, Y. H. Zhao, Y. B. Jiang, H. F. Xu, T. C. Lowe, Y. T. Zhu. Scr. Mater. 51, 225 (2004).
10. H. Miyamoto, K. Harada, T. Mimaki, A. Vinogradov, S. Hashimoto. Corr. Sci. 50, 1215 (2008).
11. L. Peguet, B. Malki, B. Baroux. Corr. Sci. 49, 1933 (2007).
12. J. G. Brunner, J. May, H. W. Höppel, M. Göken, S. Virtanen. Electrochim. Acta. 55, 1966 (2010).
13. N. A. Amirkhanova, R. Z. Valiev, I,V. Alexandrov, R. K. Islamgaliev, Yu. B. Kutnyakova, S. L. Adasheva, E. Yu. Chernyaeva, A. G. Balyanov, A. T. Dautova, R. R. Khaydarov. USATU Herald. 7 (3), 42 (2006) (in Russian) [Н. А. Амирханова, Р. З. Валиев, И. В. Александров, Р. К. Исламгалиев, Ю. Б. Кутнякова, С. Л. Адашева, Е. Ю. Черняева, А. Г. Балянов, А. Т. Даутова, Р. Р. Хайдаров. Вестник УГАТУ. 7 (3), 42 (2006).]
14. M. M. Sharma, C. W. Ziemian. J. Mat. Eng. Perf. 17, 870 (2008).
15. M. F. Naeini, M. H. Shariat, M. Eizadjou. J. All. Comp. 509, 4696 (2011).
16. M. Hockauf, L. W. Meyer, D. Nickel, G. Alisch, T. Lampke, B. Wielage, L. Krüger. J. Mater. Sci. 43, 7409 (2008).
17. T. C. Tsai, T. H. Chuang. Mat. Sci. Eng. A. 225, 135 (1997).
18. K. G. Krishna, K. Sivaprasad, T. S. N. S. Narayanan, K. C. H. Kumar. Corr. Sci. 60, 82 (2012).
19. P. A. Khaimovich. Prob. Atomic Sci. Tech. 4, 28 (2006).
20. Y. S. Li, N. R. Tao, K. Lu. Acta Mat. 56, 230 (2008).
21. S. V. Krymskiy, E. V. Avtokratova, M. V. Markushev, M. Yu. Murashkin, O. Sh. Sitdikov. Mater. Sci. Forum. 667, 925 (2011).
22. S. V. Krymskiy, O. Sh. Sitdikov, E. V. Avtokratova, M. Yu. Murashkin, M. V. Markushev. Rev. Adv. Mat. Sci. 31, 145 (2012).
23. S. V. Krymskiy, E. V. Avtokratova, O. Sh. Sitdikov, A. V. Mikhaylovskaya, M. V. Markushev. Phys. Met. Metallogr. 226, 676 (2015).
24. E. Avtokratova, S. Krymskiy, A. Mikhaylovskaya, O. Sitdikov, M. Markushev. Mater. Sci. Forum. 838, 367 (2016).
25. S. V. Krymskiy, R. R. Ilyasov, E. V. Avtokratova, O. Sh. Sitdikov, M. V. Markushev. Prot. Met. Phys. Chem. Surf. 53, 1091 (2017).
26. N. Rangaraju, T. Raghuram, B. V. Krishna, K. P. Rao, P. Venugopal. Mat. Sci. Eng. A. 398, 246 (2005).
27. F. J. Humphreys, M. Hatherly. Recrystallization and related annealing phenomena. Oxford, Elsevier. (2004) 658 p.
28. Y. Shi, Q. Pan, M. Li, X. Huang, B. Li. J. All. Comp. 612, 42 (2014).